ICES Journal of Marine Science

ICES Journal of Marine Science (2017), 74(4), 941–954. doi:10.1093/icesjms/fsw213

Contribution to Special Issue: 'Towards a Broader Perspective on Ocean Acidification Research Part 2'

Editor's Choice

Metabolic cost of calcification in bivalve larvae under experimental ocean acidification

Christina A. Frieder, Scott L. Applebaum, T.-C. Francis Pan, Dennis Hedgecock, Donal T. Manahan*

Department of Biological Sciences, University of Southern California, Los Angeles, CA 90089-0371, USA

**Corresponding author: tel: (213) 740-5793; fax (213) 740-8123; e-mail:manahan@usc.edu*

Frieder, C. A., Applebaum, S. L., Pan, T.-C. F., Hedgecock, D., Manahan, D. T. Metabolic cost of calcification in bivalve larvae under experimental ocean acidification. – ICES Journal of Marine Science, 74: 941–954.

Received 21 July 2016; revised 24 October 2016; accepted 25 October 2016; advance access publication 9 December 2016.

Physiological increases in energy expenditure frequently occur in response to environmental stress. Although energy limitation is often invoked as a basis for decreased calcification under ocean acidification, energy-relevant measurements related to this process are scant. In this study we focus on first-shell (prodissoconch I) formation in larvae of the Pacific oyster, *Crassostrea gigas*. The energy cost of calcification was empirically derived to be $\leq$ 1.1 μJ (ng $CaCO_3$)$^{-1}$. Regardless of the saturation state of aragonite (2.77 vs. 0.77), larvae utilize the same amount of total energy to complete first-shell formation. Even though there was a 56% reduction of shell mass and an increase in dissolution at aragonite undersaturation, first-shell formation is not energy limited because sufficient endogenous reserves are available to meet metabolic demand. Further studies were undertaken on larvae from genetic crosses of pedigreed lines to test for variance in response to aragonite undersaturation. Larval families show variation in response to ocean acidification, with loss of shell size ranging from no effect to 28%. These differences show that resilience to ocean acidification may exist among genotypes. Combined studies of bioenergetics and genetics are promising approaches for understanding climate change impacts on marine organisms that undergo calcification.

Keywords: bioenergetics, calcium carbonate, dissolution, genetics, global change, ion transport, ocean carbonate chemistry, Pacific oyster, protein synthesis.

Introduction

During animal development major changes occur rapidly in shape and form (Thompson, 1942; Raff and Kaufman, 1991; Davidson, 2010). Many of the biological processes that regulate development and growth have substantial energy requirements. For example, protein synthesis (PS) alone can account for up to 75% of total metabolic rate in growing sea urchin larvae (Pace and Manahan, 2006) and ~50% in bivalve larvae (Lee *et al.*, 2016). Combined with other dominant processes that require energy (adenosine triphosphate; ATP)—such as the maintenance of transmembrane Na^+ gradients via ATPases—the energy requirements of developmental forms of marine invertebrates can be mostly apportioned to these two ATP-consuming processes (Leong and Manahan, 1997; Pan *et al.*, 2015).

In addition to the energy requirements for building the organic components of life, many marine organisms also produce substantial $CaCO_3$ structures that are used for morphological support, defense, and protection (Lowenstam and Weiner, 1989). The growth of these structures requires energy, but estimates of the actual amount of energy for calcification have remained elusive given the experimental challenges of separating the cellular use of the ATP pool into causative components related to calcification (Simkiss and Wilbur, 1989). Theoretical estimates for the cost of calcification range between 0.1 and 2 J (mg $CaCO_3$)$^{-1}$ (Palmer, 1992; Anthony *et al.*, 2002; Allemand *et al.*, 2011). In the case of corals, this cost of calcification is estimated to account for up to 30% of total metabolic demand (Allemand *et al.*, 2011).

Environmental perturbations can alter an organism's total demand or allocation of cellular energy (Hochachka and Somero, 2002). Shifts in allocation of energy likely impact the availability of ATP for cellular-level and whole-organism processes (Sokolova *et al.*, 2012; Applebaum *et al.*, 2014). For example, larval sea

urchins under experimental ocean acidification had an increased energy demand for PS and ion transport, while respiration rate, growth, size, and protein content remained similar relative to that of larvae in control seawater (Pan *et al.*, 2015). With regards to calcification under conditions of ocean acidification, increased energy requirements of calcification may or may not be constrained by available energy, which can be mediated by food availability (Waldbusser *et al.*, 2010; Melzner *et al.*, 2011; Thomsen *et al.*, 2013).

The investment of energy to calcification facilitates biological control of the process. Biological control can act by delineating specific regions and co-opting specific cell types to mediate shell mineralization (Mount *et al.*, 2004; Johnstone *et al.*, 2015). Modification of chemistry at the site of calcification and synthesis of an organic matrix also act as mediators of mineralization (Belcher *et al.*, 1996; Mann, 2001; Mao *et al.*, 2016). Once calcified material is formed it is often protected from bulk seawater by organic layers (e.g. the periostracum). Formed $CaCO_3$ surfaces may, however, undergo dissolution if they are in direct contact with fluids, including extrapallial fluid, that are undersaturated with respect to the $CaCO_3$ polymorph (Melzner *et al.*, 2011; Heinemann *et al.*, 2012). The rate of accretion of calcified mass is a balance between gross calcification and dissolution rates. Methods to isolate these two contrasting processes are technically challenging, and the lack of such measurements has complicated the identification of the mechanisms by which changes in carbonate chemistry alter the accretion of calcified mass (Andersson and Gledhill, 2013).

The process of calcification has a deep evolutionary history (Lowenstam and Margulis, 1980) and has been studied extensively (Simkiss and Wilbur, 1989; Mount *et al.*, 2004; Johnstone *et al.*, 2015). Of the seven different taxonomic classes of Mollusca, five are shell-bearing (Lowenstam and Weiner, 1989). The fossil record of mollusc shells dates back to the early Cambrian, over 540 million-years-ago (Ponder and Lindberg, 2008). Yet despite the vast morphological variety of molluscan adult shells and the more than 200 000 extant species, there appears to be a deep conservation of early developmental programming associated with the initiation of shell construction (Kniprath, 1981). Much less is known about the physiology of calcification in developmental stages. During the trochophore stage of molluscan development contact between endoderm and dorsal ectoderm induces shell gland formation, and first calcification occurs in an extracellular space (Hohagen and Jackson, 2013). Although adult mollusc shell is comprised of calcite or aragonite, or both, larval shells of molluscs contain aragonite (e.g. oyster: Stenzel, 1963, 1964). Developmental stages of molluscan larvae are good experimental model organisms for the study of calcification processes. Within the first 2-d post-fertilization, as we show in this study, larvae of *Crassostrea gigas* accrete more than six times their organic mass as shell mass, mainly as aragonitic calcium carbonate (Stenzel, 1964). Moreover, first-shell formation is sensitive to ocean acidification (Thomsen *et al.*, 2015). The shell is appreciably smaller with decreasing aragonite saturation state (Waldbusser *et al.*, 2014), yet whether reduced calcification is driven by a reduction in carbonate substrate availability (i.e. saturation state) or other alterations in carbonate chemistry (i.e., increased proton concentrations), which are not mutually exclusive, is under debate (Cyronak *et al.*, 2016a,b; Waldbusser *et al.*, 2016b).

Coastal acidification has had negative effects on shellfish aquaculture: larval production of the Pacific oyster *C. gigas* in commercial hatchery operations was positively correlated with $\Omega_{aragonite}$ of waters in which larval oysters were reared for the first 48 h of development (Barton *et al.*, 2012). Remediation through carbonate chemistry treatment systems has proven effective for augmenting continued larval production efforts (Barton *et al.*, 2015). Yet, given future trajectories for rates of ocean acidification, an improved understanding of calcification physiology could contribute to the adaptability of the shellfish aquaculture industry. For trochophore larvae, a non-feeding bivalve larval stage that primarily relies on maternally endowed energy (Gallager and Mann, 1986; Moran and Manahan, 2004), insufficient energy availability has been hypothesized as a mechanism by which first larval shells are smaller and malformed at low aragonite saturation (Waldbusser *et al.*, 2013, 2016a,b).

To assess the effects of changes in carbonate chemistry on the formation of the first shell (prodissoconch I) in early stages of development of the Pacific oyster, *C. gigas*, we studied the processes of calcification by incorporating measurements of shell accretion (mass change) with rates of calcification and dissolution. To consider the calcification process in the context of the larval energy budget, we measured the total energy required to complete larval development during first-shell formation. Additionally, total energy was partitioned to PS and sodium-potassium transport (*in vivo* activity of Na^+,K^+-ATPase). From these analyses, we derived an upper limit for the energy cost of calcification. Furthermore, biological variation in calcification rates of shell among different larval families of pedigreed crosses was assessed to test possible genetic effects for adaptation potential to ocean change.

Methods

Broodstock and larval culturing

Multigenerational, pedigreed genetic lines of *C. gigas* were used to make larval families from controlled male-by-female crosses. The adults used in these crosses were from a breeding programme of two to five generations, with pedigrees confirmed by DNA analyses (Hedgecock and Davis, 2007; Sun *et al.*, 2015). A total of nine larval families (Table 1) were established to maximize the possibility of obtaining contrasting phenotypes. For each family, fertilized eggs were stocked at 15 embryos ml^{-1} in two replicate 200-l culture vessels per seawater treatment (control and aragonite undersaturation). All cultures were kept in a temperature controlled room at 25°C; the seawater salinity was 33.3.

Carbonate chemistry manipulation

Prior to stocking fertilized eggs in culture vessels, the aragonite saturation state in the culture seawater was manipulated by aeration with defined concentrations of CO_2 and maintained by constant bubbling of the appropriate gas mixture during the experiment. Total dissolved inorganic carbon (DIC) and pCO_2 were measured daily in each culture vessel. DIC and pCO_2 measurements were made on a system similar to that described by Bandstra *et al.* (2006), modified for discrete samples by Hales *et al.* (2005). DIC measurements were calibrated with Certified Reference Material obtained from the Marine Physical Laboratory at Scripps Institution of Oceanography. The pCO_2 measurements were calibrated with three gas standards (200, 500, and 1200 ppm) obtained from Scott-Marrin Inc. Carbonate chemistry parameters were calculated from DIC and pCO_2 at experimental temperature and salinity using the

Table 1. Experimental conditions used to culture larvae of the Pacific oyster, *C. gigas*, at control (average conditions $\Omega_{Arag} = 2.77$) and aragonite undersaturation (average conditions $\Omega_{Arag} = 0.77$).

Trial	Family	Ω_{Arag}	$[HCO_3^-]/[H^+]$	pCO_2	pH	Dev. rate	Shell length	Shell mass	Prot.	Lipid	Resp.	Calc. onset	Calc. rate	Diss. rate	PS and NKA
a	6 (1 × 1)	2.87 ± 0.06	0.187 ± 0.004	441 ± 18	8.01 ± 0.01	X	X								
		0.84 ± 0.09	0.054 ± 0.006	2188 ± 279	7.39 ± 0.05	X	X								
a	2 (1 × 2)	2.94 ± 0.08	0.192 ± 0.006	423 ± 20	8.03 ± 0.01	X	X		X	X	X		X		X
		0.78 ± 0.02	0.050 ± 0.001	2381 ± 97	7.36 ± 0.01	X	X		X	X	X		X		X
a	8 (2 × 1)	2.89 ± 0.02	0.187 ± 0.003	428 ± 7	8.02 ± 0.00	X	X		X		X	X	X		X
		0.83 ± 0.08	0.054 ± 0.004	2193 ± 140	7.39 ± 0.03	X	X		X		X	X	X		X
a	1 (2 × 2)	2.97 ± 0.07	0.192 ± 0.006	424 ± 16	8.03 ± 0.02	X	X								
		0.88 ± 0.04	0.057 ± 0.003	2058 ± 124	7.42 ± 0.02	X	X								
b	3 (3 × 4)	2.72 ± 0.07	0.183 ± 0.004	434 ± 12	8.01 ± 0.01	X	X	X	X		X	X	X		X
		0.75 ± 0.07	0.050 ± 0.005	2295 ± 237	7.37 ± 0.04	X	X	X	X		X	X	X		X
b	4 (3 × 5)	2.61 ± 0.07	0.177 ± 0.005	458 ± 18	7.99 ± 0.01	X	X	X	X			X	X		
		0.76 ± 0.11	0.051 ± 0.008	2270 ± 363	7.37 ± 0.06	X	X	X	X			X	X		
b	9 (3 × 6)	2.66 ± 0.03	0.181 ± 0.002	443 ± 3	8.00 ± 0.00	X	X	X				X	X	X	
		0.67 ± 0.07	0.045 ± 0.005	2613 ± 272	7.31 ± 0.04	X	X	X				X	X	X	
c	7 (7 × 8)	2.72 ± 0.06	0.169 ± 0.003	430 ± 1	8.00 ± 0.00	X	X	X		X		X	X		
		0.71 ± 0.11	0.045 ± 0.007	2403 ± 440	7.34 ± 0.07	X	X	X		X		X	X		
d	5 (5 × 2)	2.68 ± 0.07	0.163 ± 0.004	426 ± 9	7.99 ± 0.01		X	X			X				
		0.75 ± 0.01	0.045 ± 0.000	2355 ± 6	7.34 ± 0.00		X	X			X				

Experiments were conducted across four trials (a–d). ANOVA of shell length between Trial-a and Trial-b confirmed there was no significant trial or trial-by-environment effect (trials pooled, Table 2). There were two replicate culture vessels per treatment per family. Average conditions ± *SD* of aragonite saturation (Ω_{Arag}), the substrate-inhibitor ratio ($[HCO_3^-]/[H^+]$), partial pressure of carbon dioxide (pCO_2; µatm) and pH (reported on the total scale) are calculated from discrete samples taken daily or once every other d from each replicate culture vessel. Temperature was maintained at 25 °C; salinity was 33.3. Response measurements made on each family are indicated by an "X" and include developmental rate (Dev. rate), shell length, shell mass, total protein content (Prot.), lipid class content, respiration rate (Resp.), onset of calcification (Calc. onset), calcification rate (Calc. rate), dissolution rate (Diss. rate), protein synthesis (PS) rate, and *in vivo* Na^+, K^+-ATPase (NKA). Family numbers are arbitrarily labelled 1–9 to correspond to the rankings given in Figure 1c, along with the parental lines used for crosses (in parenthesis). For example, larval family 2 (1 × 2) was the result of crossing an individual male and female from lines "1" and "2", respectively.

"Seacarb" package in R, parameterized as recommend (Dickson *et al.*, 2007).

Two target seawater treatments were selected to generate phenotypic contrasts in shell mass—referred to herein as control ($\Omega_{aragonite} \gg 1$) and aragonite undersaturation ($\Omega_{aragonite} < 1$). Average (± *SD*) control and aragonite undersaturation treatments across all larval families was 2.77 ± 0.13 and 0.77 ± 0.07, respectively (Table 1). Although shell length negatively correlates with aragonite saturation state (Waldbusser *et al.*, 2014, 2015) other aspects of carbonate chemistry variation could be a causative agent of the observed effect (specifically, the substrate-inhibitor ratio, Thomsen *et al.*, 2015). Calculated $[HCO_3^-]/[H^+]$ are given for each treatment in Table 1, but aragonite saturation states are referred to throughout the text for consistency.

Whole-organism measurements

Larval cultures were subsampled multiple times from 10 to 48 h post-fertilization to measure physiological and biochemical changes during first-shell formation (prodissoconch I) and prior to reaching the larval feeding stage. At each sampling interval, larvae from each 200-l culture vessel were filtered on to a mesh sieve, resuspended in ~50 ml of treatment seawater, and enumerated. Care was taken to maintain seawater carbonate chemistry treatment conditions during enumeration and *in vivo* assays. The specific set of measurements made on each larval family is listed in Table 1. From each replicate culture vessel and aragonite saturation treatment, 50 larvae were photographed at multiple stages through development with a camera mounted on a compound microscope. Images were analysed using ImageJ (NIH) to enumerate larval developmental stage and to measure shell length of veligers. Developmental rate from trochophore to veliger stage was assessed as the hour post-fertilization at which half of the larval population within a replicate culture vessel had reached the veliger stage, as evidenced by the visual presence of a shell. Shell length was measured as the longest anterior to posterior dimension of the shell parallel to the hinge line. Aliquots of larvae were frozen at −80 °C for later analysis of shell mass, protein content, and lipid class content. Shell mass was quantified as the organic-mass-free, dry-ash mass (His and Maurer, 1988; Jaeckle and Manahan, 1989; Hoegh-Guldberg and Manahan, 1995). Since the goal of this part of the study was to measure shell mass (not total organic mass), larvae were rinsed three times with deionized (Nanopure) water to remove salts, and a known number transferred to a pre-ashed, pre-weighed aluminum container. Samples were dried to constant mass (5 h at 60 °C), ashed at 450 °C for 12 h, and the mass measured on a mass-calibrated electrobalance to a sensitivity of 0.1 µg (Cahn Model 29). Additional samples were also taken at 5, 7, 11, and 17-d post-fertilization from seawater control conditions to derive a relationship between shell length and shell mass. Larval protein content was determined using the Bradford dye-binding assay, modified for developing invertebrates (Jaeckle and Manahan, 1989). Larval lipid class analysis was measured with chromatography and detected by flame ionization (Iatroscan MK-5) (Moran and Manahan, 2004).

Net calcification and dissolution rates

To determine the time post-fertilization at which there was first measurable onset of calcification, ~20000 trochophore larvae (exact number known in each experiment) were incubated in 10 ml of filtered seawater containing 8 kBq ^{45}Ca (Perkin-Elmer Inc.). A 1-ml subsample of seawater containing larvae was taken every 30 min during a 6-h time-course experiment. Larvae were vacuum-filtered onto a membrane (pore-size 8 μm; Nucleopore) and rinsed with filtered seawater to remove excess radioactivity. The organic fraction of larvae was solubilized for 24 h (Solvable; PerkinElmer Inc.). The solubilized organic fraction in the supernatant was removed and the remaining shells were triple rinsed with deionized water. Shells were then dissolved in acid (0.5 M HCl) and transferred to liquid scintillation vials containing 4 ml of scintillation cocktail (Ultima Gold^{TM}; Perkin Elmer). The amount of ^{45}Ca radioactivity in each sample was measured by liquid scintillation counting (Beckman LS 6000SC), and the amount of radioactivity corrected for the specific activity of ^{45}Ca in the seawater used for experiments. To determine the onset of calcification as measured by the appearance of ^{45}Ca in shell material, a step-by-step sequential linear regression analysis was applied to the data (^{45}Ca vs. time) until a statistically significant, positive slope was obtained. This time point represented the h post-fertilization when a measurable rate of calcification was initiated.

The rate of calcification (ng $CaCO_3$ larva^{-1} h^{-1}) for each larval family was determined based on the rate of incorporation of ^{45}Ca into shell as described earlier, except subsamples were collected every 30 min for 3 h. Calcification assays were conducted on larvae that were between 20- and 40-h post-fertilization. Rates of calcification were calculated from the slope of the linear regression analysis describing the relationship between the amount of newly calcified shell and incubation time. Preliminary tests of abiotic adsorption of ^{45}Ca to shells of dead (bleach-killed) larvae was confirmed to be <5%.

Rates of shell dissolution were determined as the loss of ^{45}Ca from the shells of live larvae. For these assays, known numbers of larvae were incubated in ^{45}Ca seawater for 4 h and then resuspended in 10 ml of ^{45}Ca-free seawater. Every 2 h during an 8-h time-course experiment, subsamples of larvae were processed following the same protocol as the ^{45}Ca assays described earlier. Dissolution rate data are expressed as the percent loss of ^{45}Ca with time. A series of four replicate dissolution assays were carried out on a given larval family that was exposed to both treatments. ANCOVA revealed no difference among dissolution assays within a treatment and replicate assays were pooled [calcium carbonate accumulation was the dependent variable, assay was the independent variable, and incubation time was the covariate (within control: $F_{3,17} = 0.06$, $p = 0.98$; within aragonite undersaturation: $F_{3,15} = 1.91$, $p = 0.19$)].

Respiration

Oxygen consumption rate was quantified with a modified micro-Biological-Oxygen-Demand method (details in Marsh and Manahan, 1999). Known numbers of larvae (between 800 and 1200, depending on stage of development) from each seawater treatment were placed in μBOD vials of known volume (precalibrated ~0.5 ml), with oxygen-saturated filtered seawater. Larvae were held in vials for 3–4 h at 25°C ($N = 7$–10 independent respiration vials per replicate culture). The amount of oxygen consumed was measured with calibrated polarographic oxygen sensors (Strathkelvin, Inc. Model 130) at the end of each incubation period. Oxygen consumption rates were corrected for background oxygen consumption, which was on average 20% of total oxygen consumption at the high temperatures used in these experiments for larvae of *C. gigas* (25°C).

In vivo Na^+,K^+-ATPase activity

The physiologically active fraction of total Na^+,K^+-ATPase was measured by quantifying the *in vivo* rate of $^{86}Rb^+$ transport, a physiological analog for potassium transport by cells. The application of this assay in marine invertebrate larval forms has been described in detail by Leong and Manahan (1997) and Pan *et al.* (2016). Briefly, a known number of larvae was placed in 10 ml of filtered seawater to which was added 0.9 MBq of $^{86}Rb^+$ (PerkinElmer Inc.). During a 16-min time-course experiment, a 1-ml subsample of individuals was removed from the seawater every 2 min, collected on a filter membrane, and rinsed with filtered seawater to remove excess $^{86}Rb^+$. The membrane filter holding the biological sample was solubilized overnight, liquid scintillation cocktail was added, and the amount of radioactivity in each vial was determined in the same manner as described for ^{45}Ca. The rate of ion transport was calculated from the difference between the slope of the linear regression describing the relationship between $^{86}Rb^+$ transport and incubation time in the presence and absence of 2 mM ouabain, a concentration that saturates inhibition of *in vivo* Na^+,K^+-ATPase based on pre-established dose-response relationships (Pan *et al.*, 2016). To convert this value to a rate of K^+ transport (and, hence, *in vivo* Na^+,K^+-ATPase activity), the rate of $^{86}Rb^+$ transport was corrected for the specific activity of K^+ in seawater. The physiologically active fraction of total Na^+,K^+-ATPase is reported as pmoles of inorganic phosphate larva^{-1} h^{-1}.

Absolute rates of protein synthesis (PS)

Rates of PS were determined following methods described for larval stages of *C. gigas* (Lee *et al.*, 2016). The *in vivo* measurement of PS relies on the uptake of a radiolabelled amino acid by larvae from seawater and incorporation of that radiolabelled amino acid into nascent protein. Soon after fertilization, eggs of *C. gigas* activate a capacity to transport amino acids directly from seawater (Manahan, 1983a). Such active transport continues throughout larval development, where the primary site of uptake is the velum (Manahan, 1983b; Manahan and Crisp, 1983), and in adult stages, where the primary site of uptake is the gill (Pequignat, 1973; Manahan *et al.*, 1982; Wright and Secomb 1986). Approximately 10 000 larvae (exact number known in each experiment) were incubated in 10 ml of filtered seawater containing 74 kBq ^{14}C-glycine (Perkin-Elmer Inc.). The final amino acid concentration was 10 μM glycine (adjusted by the addition of non-radioactive "cold carrier" glycine; Sigma-Aldrich). During a ~30-min time-course experiment, a series of 1-ml subsamples of individuals in seawater was collected every 6 min. Each sample was vacuum filtered onto a filter membrane (as described earlier), rinsed with filtered seawater to remove excess ^{14}C, and frozen at −80 °C until further analysis. The amount of ^{14}C-glycine incorporated into trichloroacetic acid-precipitable protein at each time interval was measured by scintillation counting. The amount of ^{14}C-glycine incorporated into protein was corrected for the change in the intracellular specific activity of ^{14}C-glycine in the free amino acids pool of larvae (analytical details and calculation

of synthesis rates in Lee *et al.*, 2016). The amount of total glycine incorporated into protein was converted to an absolute rate of PS. This calculation was based on the amino acid composition of the whole-body protein content of *C. gigas* (Lee *et al.*, 2016). For the samples used in this study, the mole-percent amino acid composition of whole-body protein in trochophore and newly-formed D-veliger stage larvae was measured (UC Davis Proteomics Core at the Genome Center). The measured mole-percent-corrected molecular mass of amino acids in protein is 126.9 ± 0.3 g mole^{-1}, and the mole-percent of glycine is 11.6 ± 0.04%. ($N = 3$ ± SE).

Allocation of metabolic energy to PS and ion transport

The proportion of metabolic energy allocated to PS was calculated using the measured energy cost per unit of protein synthesized in larvae of *C. gigas* [(Lee *et al.*, 2016); 2.1 ± 0.2 J (mg protein synthesized)$^{-1}$]. This cost was previously determined from concurrent measurements of rates of PS and oxygen consumption in the presence and absence of the PS inhibitor, emetine. In this study, the proportion of metabolic energy allocated to *in vivo* ion transport activity of Na^+,K^+-ATPase was calculated by converting values of K^+ transport to ATP equivalents (Leong and Manahan, 1997; Pan *et al.*, 2016). Respiration rates were converted to ATP equivalents using 5.2 pmol ATP (pmol O_2)$^{-1}$ (McGilvery, 1979).

Statistical analysis

To test for differences in the effect of aragonite saturation state among larval families, a mixed-effects two-factor analysis of variance was employed with larval family as the random factor and environment the fixed factor (Lynch and Walsh, 1998; Quinn and Keough, 2002). There were two large-scale, experimental replicate culture units (200-l) per each combination of carbonate chemistry treatment and family. Although experiments on the nine families were performed at different times (experimental trials listed in Table 1), there was no effect of either trial or trial-by-environment on shell length; hence, data from all trials were pooled for subsequent statistical analyses. For some response variables, multiple measurements were made on separate larvae from a single replicate culture (i.e. ~50 measurements of shell length, 3 measurements of shell mass, and 7–10 measurements of respiration rate). This is a common design for measurements of small animals in culture vessels (Hurlbert, 1984; Cornwall and Hurd, 2016). Measurements of separate larvae and pools of larvae, when applicable, were incorporated as a nested term to the linear model. Importantly, this factor became the denominator for tests of family and family-by-treatment interaction, as recommended by Quinn and Keough (2002). In the case of the calcium transport assays, an analysis of covariance was employed with hour as the covariate and larval family and environment as factors. In the case of PS and sodium-potassium transport, measurements were made at both 20- and 42-h post-fertilization on three larval families. There was no effect of treatment for 42-h-old larvae for either response variable, and so differences between treatments and among families were focused on 20-h-old larvae as this was the time period at which larvae transition from the trochophore to the veliger stage. Each response metric fulfilled assumptions of normality and homogeneity of variance.

Results

Larval shell length and mass

The shell length of 48-h-old D-stage veliger larvae of *C. gigas* is negatively impacted by aragonite undersaturation (Ω = 0.77), with an overall reduction of 18% averaged across nine families (Figure 1a). The negative impact on shell mass is much greater than on shell length; shell mass is 74 ± 4 ng larva^{-1} under control conditions ($\Omega = 2.77$), reducing to 32 ± 4 ng larva^{-1} at aragonite undersaturation (average ± SE; Figure 1b). For the different larval families tested, there is a significant family-by-environment interaction on shell length (Table 2). Shell length in one of the nine larval families tested is not impacted by aragonite undersaturation (Family 1, 2 × 2: a non-significant 3-μm decrease in shell length relative to control conditions). The reduction in shell length in the remaining eight larval families range from 9 to 21 μm, a reduction of 12–28% relative to control larvae (Figure 1c). Family 8, the 2 × 1 hybrid was one of the most sensitive families to aragonite undersaturation, more sensitive even than its 1 × 1 inbred parent (Family 6) and more so than the reciprocal hybrid 1 × 2 (Family 2).

Developmental progression from trochophore-to-veliger stage

Approximately 50% of developing larvae reach the D-veliger stage by 17-h post-fertilization under control conditions; this rate of

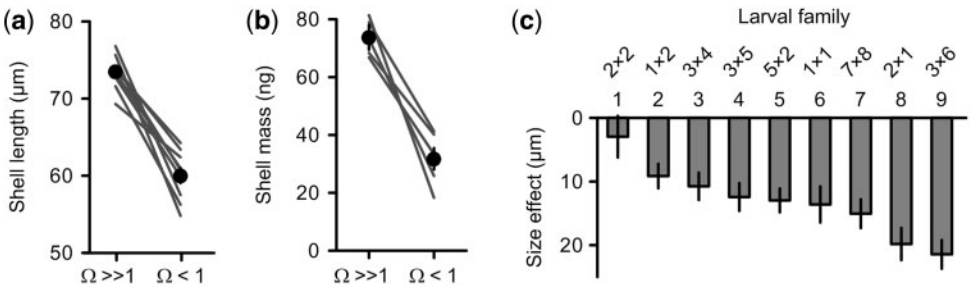

Figure 1. (a) Shell length (μm) and (b) shell mass (ng) at 48-h post-fertilization in larvae of *C. gigas* cultured under control conditions ($\Omega \gg 1$ at 2.77) and at aragonite undersaturation ($\Omega < 1$ at 0.77). Data plotted as the average value ± SE of all larval families (black circles). Fitted lines represent individually tested larval families. Nine larval families are shown for shell length and five for shell mass. (c) The difference between the means of shell length (± 95% *CI*) at aragonite undersaturation vs. control conditions across nine larval families, ranked by effect (Family 1 < Family 2–7 < Family 8–9). Genetic crosses are given earlier for each larval family (male-by-female crosses of pedigreed lines).

Table 2. Results of two-way analysis of variance of larval family-by-environment under a mixed model: larval family treated as a random factor, and saturation state (Ω) treated as a fixed factor.

Response	Source	*df*	MS	*F* Ratio	Probability > *F*
Shell length					
	$\Omega_{Aragonite}$	1	96 226	69.2	**<0.0001**
	Family	8	800	1.65	0.18
	Ω × family	8	1391	2.87	**0.03**
	Replicate (Ω-Family)	18	484	19.4	**<0.001**
	Residuals	2121	25		
Shell mass					
	$\Omega_{Aragonite}$	1	26 477	47.2	**0.002**
	Family	4	272	0.50	0.74
	Ω × Family	4	561	1.04	0.44
	Replicate (Ω-family)	10	542	8.46	**<0.0001**
	Residuals	41	64		
Developmental rate					
	$\Omega_{Aragonite}$	1	219	26.6	**0.004**
	Family	5	16.5	3.64	**0.03**
	Ω × family	5	8.2	1.82	0.18
	Residuals	12	4.5		
Calcification onset					
	$\Omega_{Aragonite}$	1	6.61	20.0	**0.01**
	Family	4	0.67	4.12	**0.03**
	Ω × family	4	0.33	2.04	0.16
	Residuals	10	0.16		
Calcification rate					
	$\Omega_{Aragonite}$	1	215	12.8	**0.02**
	Family	5	37	2.2	0.20
	Ω × Family	5	17	14	**<0.0001**
	hpf (Covariate)	1	286	240	**<0.0001**
	Residuals	218	260		
Respiration rate, 20 hpf					
	$\Omega_{Aragonite}$	1	2.83	6.24	0.13
	Family	2	10.7	4.29	0.10
	Ω × Family	2	0.45	0.18	0.84
	Replicate (Ω-Family)	4	2.49	1.13	0.35
	Residuals	95	2.21		
Protein synthesis, 20 hpf					
	$\Omega_{Aragonite}$	1	0.002	0.14	0.74
	Family	2	0.073	3.41	0.10
	Ω × Family	2	0.013	0.62	0.57
	Residuals	6	0.022		
In vivo Na^+,K^+-ATPase, 20 hpf					
	$\Omega_{Aragonite}$	1	138	10.4	0.08
	Family	2	3.3	1.5	0.30
	Ω × Family	2	13.2	6.0	**0.04**
	Residuals	6	2.2		
Allocation of ATP to protein synthesis, 20 hpf					
	$\Omega_{Aragonite}$	1	24	0.53	0.54
	Family	2	263	3.21	0.11
	Ω × Family	2	46	0.56	0.60
	Residuals	6	82		
Allocation of ATP to In vivo Na^+,K^+-ATPase, 20 hpf					
	$\Omega_{Aragonite}$	1	918	7.52	0.11
	Family	2	24	1.42	0.31
	Ω × Family	2	122	7.36	**0.02**
	Residuals	6	17		

Shell length and mass were measured at ~48-h post-fertilization. Developmental rate is the h at which 50% of the larval population had reached veliger stage, as determined by light microscopy observation. Calcification onset is the h at which accumulation of shell was detectable by ^{45}Ca transport. Some response measurements (e.g. respiration rate) were made on multiple, separate pools of larvae within a replicate culture vessel. When applicable, replicate was incorporated as a nested term to the mixed model [Replicate (Ω-Family)]. Environmental conditions and larval families included in each analysis are provided in Table 1. Hours post-fertilization, *hpf*.

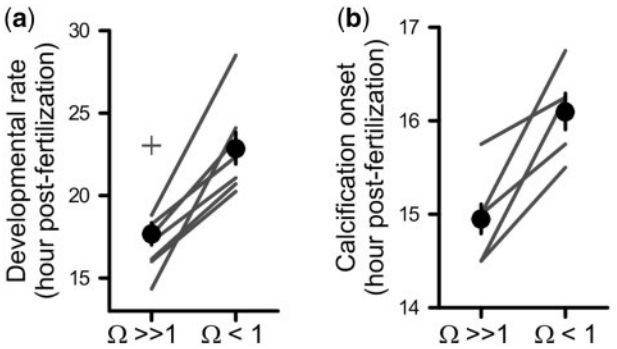

Figure 2. (a) The time to D-hinge, measured as the time (h) post-fertilization at which half of the larval population reached the veliger stage for larvae of *C. gigas* exposed to control conditions ($\Omega \gg 1$) and aragonite undersaturation ($\Omega < 1$). One family did not develop to the veliger stage by 48 h post-fertilization (cross symbol). (b) Timing of calcification, measured as the h post-fertilization at which there was significant incorporation of ^{45}Ca into the larval shell fraction, for larvae exposed to control and aragonite undersaturation conditions. Data are plotted as the average value ± *SE* of all larval families (black circles). Lines represent individual tested larval families. Eight families were measured for developmental rate, and five families measured for calcification onset.

development is delayed by 6 h at aragonite undersaturation (Figure 2a). There is difference in the timing of development among different larval families (Table 2). Notably, one family does not reach the D-veliger stage under conditions of aragonite undersaturation, further supporting a family effect (and not included in the statistical analysis presented in Table 2).

The onset of first-shell formation was measured with a highly sensitive method, using the appearance of radiolabelled calcium in the inorganic fraction of the larva. Larvae initiate calcification at 15-h post-fertilization under control conditions; at aragonite undersaturation there is a 1-h delay in the onset of calcification (Figure 2b). This latter value is much less than the observed 6-h morphological delay and equates to a 3% reduction in time available for shell accretion by 48-h post-fertilization at aragonite undersaturation relative to control conditions (i.e. 33 total h of calcification at control conditions vs. 32 h of calcification at aragonite undersaturation). For the larval families tested, there is a significant difference in the onset of calcification (Table 2); this effect, however, was minimal at less than a 2-h difference among families (Figure 2b).

Calcification and dissolution rates of initial shell formation

There was a significant difference in rates of calcium uptake into shell during ^{45}Ca assays at control and aragonite undersaturation (e.g. Family 3; Figure 3a). On average there was a 64% reduction, 0.59 vs. 1.66 ng $CaCO_3$ $larva^{-1}$ h^{-1}, in calcification rate at aragonite undersaturation relative to control conditions (Figure 3b). Across six larval families, there were substantial differences in calcification rate (Table 2). At control conditions, calcification rates across families range from 0.57 ± 0.11 to 3.1 ± 0.23 ng $CaCO_3$ $larva^{-1}$ h^{-1} (± SE of slope; Figure 3b). At aragonite undersaturation, calcification rates across families ranged from 0.18 ± 0.03 to 1.2 ± 0.18 ng $CaCO_3$ $larva^{-1}$ h^{-1} (± SE of slope; Figure 3b).

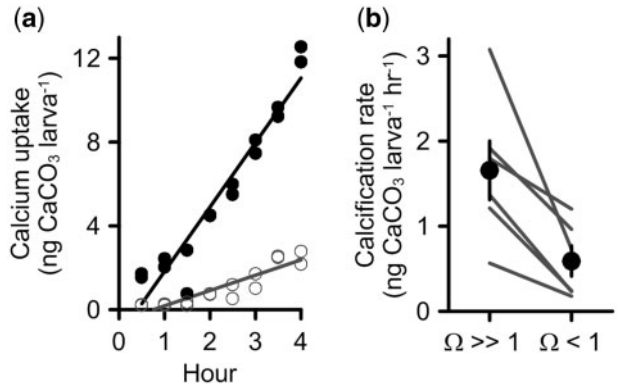

Figure 3. (a) ^{45}Ca uptake by larvae of *C. gigas* from Family 3. The accretion of calcium carbonate (ng $CaCO_3$ larva^{-1}) at control (black circles) and aragonite undersaturation (open circles). Each data point represents a different subsample of larvae. Two assays per control and aragonite undersaturation were combined after ANCOVA confirmed no difference in slope or intercept. (b) Mean ($\pm SE$; black circles) net calcification rate (ng CaCO3 larva^{-1} h^{-1}) at control conditions ($\Omega \gg 1$ at 2.77) and aragonite undersaturation ($\Omega < 1$ at 0.77) averaged across six different larval families (black lines).

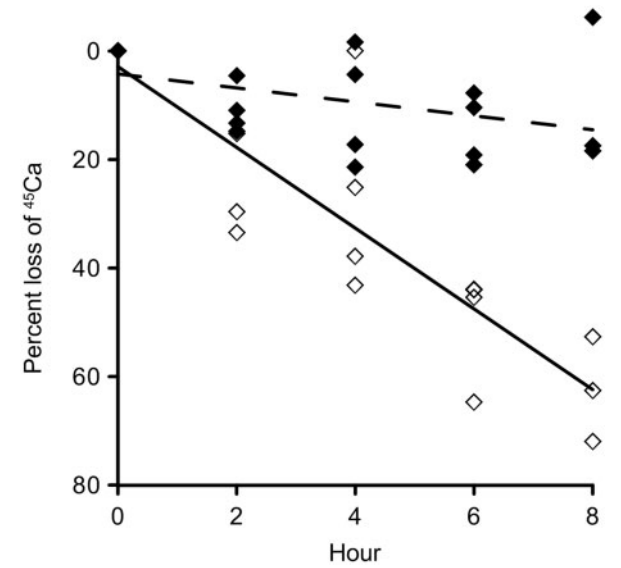

Figure 4. Percent loss of ^{45}Ca from shells of live larvae of *C. gigas* exposed to control ($\Omega \gg 1$ at 2.77; solid symbols) and aragonite undersaturation ($\Omega < 1$ at 0.77; open symbols) conditions. Prior to measurement of dissolution rate, larvae were incubated for 4 h in ^{45}Ca-labelled seawater. Four separate 8-h time-course assays (including time zero) were conducted per treatment and combined after ANCOVA confirmed no difference in slope or intercept. At control conditions, there was no change in ^{45}Ca (linear regression: $F_{1,17} = 3.48$; $p = 0.08$). At aragonite undersaturation, ^{45}Ca from the shell decreased at a rate of 7.6% per h (percent loss = −4.18 − 7.6 × hour: $F_{1,15} = 110$; $p < 0.0001$).

The rate of shell dissolution was measured as the loss of ^{45}Ca from shells of live larvae after the larvae had been incubated for 4 h in the presence of ^{45}Ca. At control conditions, dissolution is not apparent (linear regression: $F_{1,17} = 3.48$; $p = 0.08$) (Figure 4). In contrast, at aragonite undersaturation dissolution is significant: larvae lost ^{45}Ca from the shell at a rate of 7.6% h^{-1} (percent loss = −4.18–7.6 × h: $F_{1,15} = 110$; $p < 0.0001$). As a result, net and gross calcification rates of larvae at aragonite undersaturation are not equivalent and, hence, the rate of ^{45}Ca accumulation in shell is a measure of the net calcification rate, not gross calcification rate.

Together, a reduction in calcification and measurable dissolution account for the 57% reduction in the mass of shell accreted at aragonite undersaturation. Although dissolution was apparent at aragonite undersaturation, the primary mechanism was the reduction in calcification rate. The average rate of net calcification (i.e. the balance between gross calcification and dissolution rate, Figures 3 and 4) was 1.66 ± 0.35 ng larva^{-1} h^{-1} at control conditions; this rate decreased to 0.59 ± 0.18 ng larva^{-1} h^{-1} at aragonite undersaturation (Figure 3). This decrease equates to 47 ng of $CaCO_3$ over 33 h that is not accreted at aragonite undersaturation. The result would be a shell mass of only 27 ng (74 ng minus 47 ng), a value that is in close agreement with the gravimetrically measured shell mass of 32 ± 4 ng at aragonite undersaturation (Figure 1b).

Energy demand and energy allocation during first-shell formation

Oxygen consumption rates were measured on multiple samples ($N = 105$) throughout the trochophore-to-veliger transition, 15- to 48-h post-fertilization (Figure 5a). Larvae exposed to aragonite undersaturation did not have altered rates of energy consumption relative to control conditions (Table 2). To determine the total amount of oxygen consumption during this time period, a second-order polynomial model was fit to the data from 15- to 48-h post-fertilization, regardless of carbonate chemistry treatment (O_2 consumption rate = −0.013 × Age^2 + 0.815 × Age – 4.36; root-mean-square error = 0.98; $N = 105$). From the integral of the model, total oxygen consumption during this time period was determined to be 248 pmol O_2 larva^{-1}. This oxygen demand has an energy equivalent of 120 µJ larva^{-1} [calculation based on oxidation at 484 kJ mol^{-1} O_2 (Gnaiger, 1983)].

The major biochemical reserve that is depleted during this pre-feeding developmental transition from the trochophore to the veliger stage is triacylglycerols (TAGs) (Gallager and Mann, 1986; Moran and Manahan, 2004). An energy demand of 120 µJ would require the equivalent of 3 ng lipid [based on an energy equivalent of 39.5 µJ per ng lipid (Gnaiger, 1983)]. A reduction in the content of both TAGs and phospholipids was measured between 18-h and 3-d post-fertilization. At 18 h, average TAGs content was 3.2 ± 0.4 ng larva^{-1} (±SE, $N = 4$); by 3-d post-fertilization, there was a 9-fold reduction to 0.37 ± 0.02 ng larva^{-1} (±SE, $N = 4$). Importantly, TAGs content did not differ for larvae exposed to the different seawater treatments (*t*-test: 18-h post-fertilization, $t_{0.05(2),2} = 4.88$, $p = 0.16$; 3 d, $t_{0.05(2),2} = 0.9$, $p = 0.44$). At 18 h, average phospholipid content was 1.68 ± 0.2 ng larva^{-1} ($\pm SE$, $N = 4$); by 3-d post-fertilization there was a 38% reduction to 1.05 ± 0.1 ng larva^{-1} ($\pm SE$, $N = 2$). Average protein content was 8.46 ± 0.61 ng larva^{-1} ($\pm$ *SE*, $N = 16$) and did not decrease during the period of development studied (between 15- and 40-h post-fertilization, $F_{1,10} = 0.27$, $p = 0.62$).

The allocations of ATP to the two major energy-consuming cellular processes of PS and sodium-potassium transport were

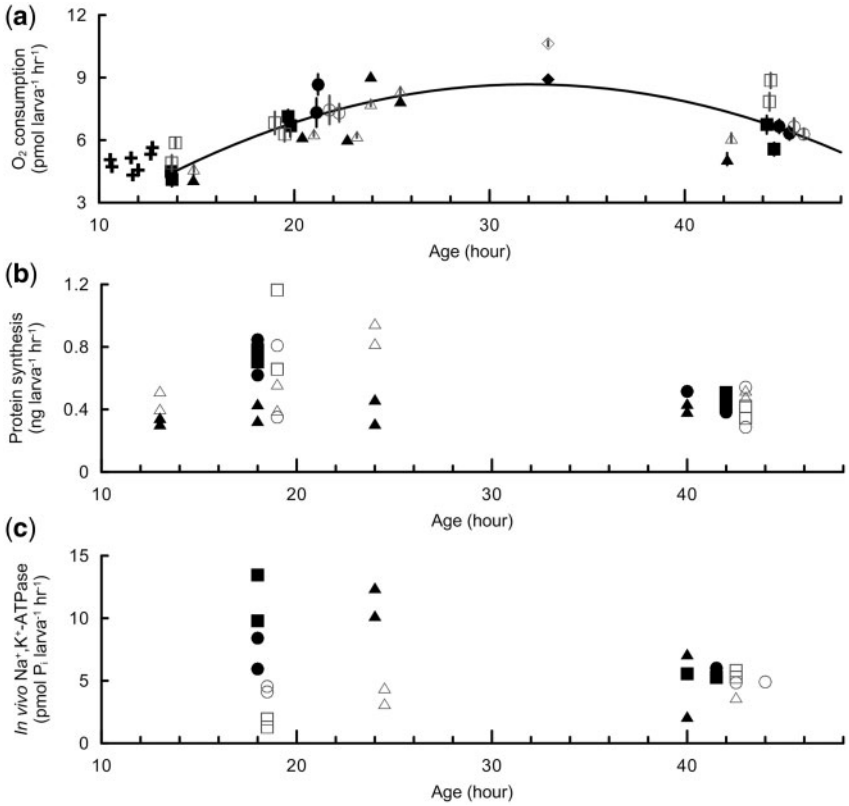

Figure 5. (a) Oxygen consumption rate (pmol O_2 larva^{-1} h^{-1}) of *C. gigas* during the trochophore-to-veliger transition at control conditions (filled) and aragonite undersaturation (open). Each data point represents the average oxygen consumption rate from 7 to 10 biological-oxygen-demand incubations initiated with larvae from a replicate culture vessel. Different symbols represent different larval families: Family 2 (circle), Family 8 (square), Family 3 (triangle), Family 5 (diamond), and cross symbols are measurements not included in the polynomial model because measurements were taken prior to the onset of calcification. Solid line is second-order polynomial model from 15- to 48-h post-fertilization, regardless of aragonite saturation treatment (root-mean-square error = 0.98). Total oxygen consumption during this time period was 248 pmol O_2 larva^{-1}. The standard error among biological-oxygen-demand respiration vials ranged from 0.01 to 0.69. (b) Absolute rates of PS in larvae of *C. gigas* exposed to control (filled) and aragonite undersaturation (open) conditions. Different symbols represent different larval families (same as in a). Each data point represents the slope of a single PS assay. (c) *In vivo* Na^+,K^+-ATPase activity in larvae of *C. gigas* exposed to control conditions and aragonite undersaturation. Data point symbols refer to different larval families (same as in panel a). For overlapping data points, offsets along the x-axis have been made for visual purposes, but at no more than 1 h.

measured to determine whether major re-allocations in cellular energy occurred to compensate for decreased calcification when larvae were exposed to the adverse carbonate chemistry condition of aragonite undersaturation. Average PS rate is 0.53 ± 0.04 ng larva^{-1} h^{-1} (grand mean ± *SE*, $N = 32$; Figure 5b). Since protein content did not change during this phase of development, a measured rate of PS was equivalent to protein turnover. Expressed as a percent of whole-body protein content, the fractional turnover rate of protein was 5.2 ± 0.4% h^{-1} (±*SE*, $N = 12$). At ~20-h post-fertilization, PS rate was measured in three larval families: there was no effect of seawater treatment or larval family on rate of PS or turnover (Table 2; Figure 5b). The amount of total ATP allocated to PS was 36 ± 2% (Figure 6b: range 17–74%, $N = 32$). Given that there was no effect of seawater treatment on PS rate or energy utilization, there was also no effect of treatment on the allocation of ATP to PS (Table 2; Figure 6b).

In contrast, sodium-potassium transport (*in vivo* Na^+,K^+-ATPase activity) decreased by 50% at aragonite undersaturation – an aragonite-by-family effect ($p = 0.04$) that was most pronounced at ~20-h post-fertilization (Table 2; Figure 5c). At this time period, sodium-potassium transport reached values as high as 10 pmol P_i larva^{-1} h^{-1} under control conditions, but only 3.3 pmol P_i larva^{-1} h^{-1} at aragonite undersaturation. In both seawater treatments, sodium-potassium transport converged to 5 pmol P_i larva^{-1} h^{-1} by the end of first-shell formation at ~40-h post-fertilization. Accordingly, at ~20-h post-fertilization, there was a decrease from 21 ($N = 6$) to 11% ($N = 6$) in the allocation of ATP to sodium-potassium transport under control and aragonite undersaturated conditions, respectively (Figure 6b). At ~20-h post-fertilization, sodium-potassium transport was measured in three larval families. There were significant family-by-environment interactions for both the rate of sodium-potassium transport ($p = 0.04$) and the allocation of ATP to this process ($p = 0.02$) (Table 2). In all larval families, sodium-potassium transport decreased under aragonite undersaturation conditions, although the magnitude of the effect differed.

Combined, PS and sodium-potassium transport accounted for ~50% of the larval rate of energy expenditure (Figure 6b). Thus, about 60 μJ (i.e. 50% of 120 μJ) of energy remained available for other ATP-consuming processes. This latter category can be used to estimate the cost of calcification.

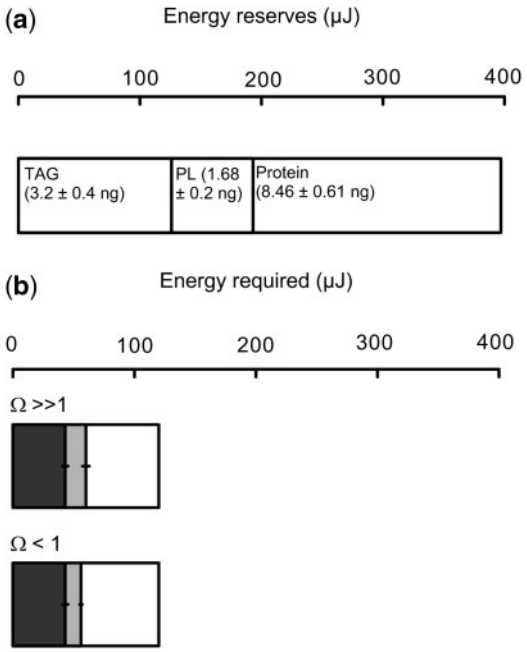

Figure 6. (a) Energy reserves (μJ) based on biochemical composition of larvae of *C. gigas* at 18-h post-fertilization for triacylglycerols (TAG), phospholipids (PL), and protein. Values in parentheses are measured amounts (±*SE*) converted to energy equivalents (μJ). There was no effect of aragonite undersaturation treatment on measured biochemical content. (b) Energy required during the trochophore-to-veliger transition. Energy equivalents (μJ) for protein synthesis (dark grey) and *in vivo* Na^+,K^+-ATPase activity (light grey) in larvae of *C. gigas* exposed to control conditions ($\Omega \gg 1$ at 2.77) and aragonite undersaturation ($\Omega < 1$ at 0.77). Energy allocated from the total ATP pool was calculated from concurrent measurements of protein synthesis, *in vivo* Na^+,K^+-ATPase, and respiration rate (Figure 5). The amount of energy remaining for other ATP-consuming processes is indicated by the white section of each horizontal stacked bar. Data plotted as the average ± *SE*.

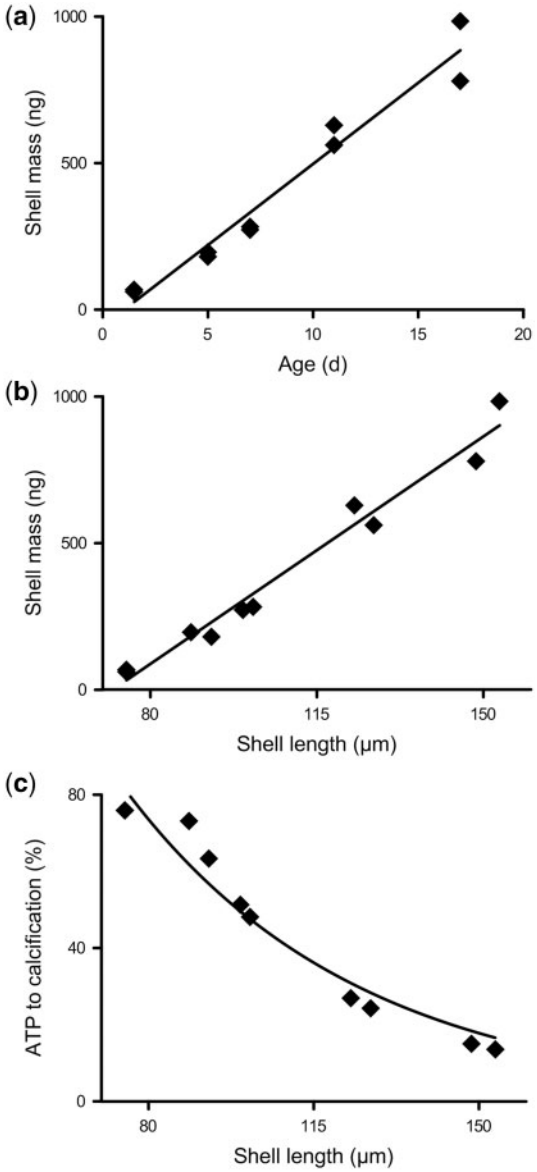

Figure 7. (a) Shell mass (ng) as a function of age (d post-fertilization) from measurements made between 2- and 17-d post-fertilization for larvae of *C. gigas* cultured at control conditions (Family 2). There is a linear relationship between shell mass and age (Shell mass = 57 × Age – 74). (b) Shell mass (ng) as a function of shell length (μm) (Shell mass = 11 × Shell length – 798). (c) The percent allocation of ATP to calcification as a function of shell length (μm). Rate of energy utilization (μJ $larva^{-1}$ h^{-1}) calculated from rates of oxygen consumption from this study (Figure 5a) and later stage larvae from Pace *et al.* (2006).

The energy cost of calcification

An upper limit for the cost of calcification can be calculated from the data given earlier. This value is based on the 60 μJ that remains from the 120 μJ, after accounting for the cost of PS and sodium-potassium transport. During this time of development, 74 ng of shell mass was accumulated (Figure 1b). Hence the cost of accreting 74 ng of shell can be derived from the 60 μJ of available energy (Figure 6b). In addition, a fraction of whole-body synthesized protein is destined for the organic matrix of shell. In general, the organic matrix constitutes 0.01–5% of shell mass (Piez, 1961). Assuming 5% of the shell is organic and most of that is protein, the energetic cost to produce 3.7 ng of protein would be 7.8 μJ [74 ng of shell × 5% protein × 2.1 μJ (ng protein synthesized)$^{-1}$]. Additionally, a fraction of Na^+,K^+-ATPase enzyme activity could be driving other membrane transport processes that directly support the calcification process. Contributing half of the ATP utilized by Na^+,K^+-ATPase to calcification, as indicated by the observed decrease in Na^+,K^+-ATPase activity at aragonite undersaturation (Figures 5c and 6b), would equate to 12.6 μJ (i.e. 120 μJ of total energy × 21% ATP allocated to Na^+,K^+-ATPase × half, the activity that may be contributing to calcification). Thus, an upper estimate for the cost of calcification is calculated to be 80.4 μJ (60 + 7.8 + 12.6) to precipitate 74 ng of $CaCO_3$ − equivalent to a cost of 1.1 J (mg $CaCO_3$)$^{-1}$.

Several of the families tested for the effect of aragonite undersaturation were grown for up to 17 days. The growth rates of larval families grown under control conditions ranged from 4.4 and 6.5 μm d^{-1} (Family 4 and 8, respectively). At aragonite undersaturation, growth rates of larval families were slower, ranging from 2.8 to 5.2 μm d^{-1} (Family 8 and Family 3, respectively). Between

2- and 17-d post-fertilization, shell mass was accreted at a linear rate of 57 ng shell larva^{-1} d^{-1} (Figure 7a), equivalent to a growth rate of 11 ng shell per µm of shell length (Figure 7b). The amount of energy allocated to the process of shell formation can be calculated as the rate of shell accretion (57 ng shell larva^{-1} d^{-1}) multiplied by the cost of calcification [1.1 µJ (ng $CaCO_3$)$^{-1}$]. This equates to a constant cost during this growth period of 63 µJ larva^{-1} d^{-1}. This allocation to calcification as a percent of total metabolism changes with shell length (Figure 7c). For fully formed-shelled larvae, the result is a reduction in the fraction of total energy allocated to calcification from ~75% to <15% in later stage larvae (Figure 7c). (*cf.* 67% for a trochophore larva to form the first shell, see "Discussion" section.)

Discussion

As an experimental organism the Pacific oyster, *C. gigas*, offers unique options for studies of the physiology of development (Pace *et al.*, 2006; Curole *et al.*, 2010; Meyer and Manahan, 2010; Lee *et al.*, 2016; Pan *et al.*, 2016). In this study, these experimental advantages include the tractability of manipulations to study calcification processes that occur very rapidly during early stages of development, and the availability of genetic pedigreed lines that permit crosses that result in contrasting phenotypes for studies of adaptation to environmental change. In general, our findings (Figure 1a) support previous work that demonstrates that shell formation in bivalves is sensitive to changes in seawater carbonate chemistry (i.e. aragonite undersaturation and the bicarbonate-to-proton ratio; Thomsen *et al.*, 2015; Waldbusser *et al.*, 2015). In our studies, there was a 57% decrease in the mass of shell accreted under aragonite undersaturation (Figure 1b: 74 ± 4 ng at control conditions; *cf.* 32 ± 4 ng at aragonite undersaturation). Notably this 57% reduction in shell mass is much greater than the 18% reduction in shell length (Figure 1a and b), demonstrating that size as a proxy of the shell underestimates the magnitude of the adverse environmental effect. Decreased calcification rates (measured with radioactive tracers) have been observed in other species of bivalve larvae in response to decreasing saturation state of aragonite (Gobler and Talmage, 2013). Combined, these observations support measurements of decreased shell thickness with increasing pCO_2 (Gaylord *et al.*, 2011). Abnormalities in shell morphology are also common at aragonite undersaturation (Kurihara *et al.*, 2007).

Energy reserves and energy requirements during early bivalve shell formation

In early stage larvae of *C. gigas*, proteins are the dominant biochemical component (60%), with TAGs (23%), and phospholipids (13%) present in lower amounts (Moran and Manahan, 2004). In this study the amount of protein in 18-h-old larvae was 8.46 ± 0.61 ng larva^{-1}, which has an energy equivalent of 204 µJ [based on 24.0 kJ (g protein)$^{-1}$ (Gnaiger, 1983)]. Protein was not depleted during the period of development studied and hence did not contribute to meeting metabolic rate ($F_{1,10} = 0.27$, $p = 0.62$). The amounts of TAGs and phospholipids in 18-h-old larvae were 3.2 ± 0.4 ng larva^{-1} and 1.68 ± 0.2 ng larva^{-1}, respectively [combined equivalent of 194 µJ based on 39.5 kJ (g lipid)$^{-1}$ (Gnaiger, 1983)]. The *actual* energy made available from the depletion of the 2.83 ng of TAGs during development was 112 µJ (calculation based on the decrease in TAGs content between 18-h and 3-d post-fertilization, i.e. 3.2−0.37 ng). A similar value for the decrease in TAGs content was observed by Moran and Manahan (2004) during early development of *C. gigas* (2.8 ng decrease between 12-h and 2-d post-fertilization). In this study, the amount of phospholipid was also observed to decrease by 0.63 ng between 18-h and 3-d post-fertilization (equivalent to 25 µJ). In comparison to the total of 137 µJ available through catabolism of TAGs (112 µJ) and phospholipid (25 µJ), the cumulative metabolic energy consumed through respiration during the developmental transition from trochophore larva to the first-shelled-veliger stage was 120 µJ. These respiration rates are, in turn, consistent with previously reported values for oxygen consumption in developmental stages of *C. gigas* (Hoegh-Guldberg and Manahan, 1995; Moran and Manahan 2004; Pace *et al.*, 2006). Hence, within reasonable experimental error (Figures 5 and 6), the energy made available through depletion of lipids (137 µJ) could fully account for the energy requirement of the developmental transition from trochophore-to-veliger larval stage (120 µJ). Furthermore, as shown by Moran and Manahan (2004), larvae of *C. gigas* are capable of maintaining metabolic rates for weeks once TAGs are depleted. Importantly, such "starved" larvae had the ability to recover and grow once fed with algae even after 17 d without food. The findings of Moran and Manahan (2004), together with the data presented in this study (Figures 5 and 6), are in contrast to other estimates that conclude that first-shell formation in bivalve larvae is energy limited by low amounts of lipid (Waldbusser *et al.*, 2013, 2016a,b; Brunner *et al.*, 2016).

Energy cost of calcification

From our empirical data (Figures 1b, 5, and 6), we derive an upper estimate for the energy cost of calcification to be 1.1 J (mg $CaCO_3$)$^{-1}$. This upper estimate is based on the energy available after accounting for energy allocated to both PS and Na^+,K^+-ATPase (Fig. 6), in addition to assuming that 5% of shell is organic (mostly protein; Piez, 1961) and that 50% of the ATP utilized by Na^+,K^+-ATPase can be attributable to ion transport processes related to calcification. We note that our empirically derived estimate of 1.1 µJ (ng $CaCO_3$)$^{-1}$ for the cost of calcification falls within the range of theoretical estimates [0.1 and 2 J (mg $CaCO_3$)$^{-1}$ (Palmer, 1992; Anthony *et al.*, 2002; Allemand *et al.*, 2011)]. For example, Palmer (1992) applied a range of values from 3.6 to 5.0 J mg^{-1} for synthesis of the protein-based organic matrix during shell formation. This value has been used to calculate theoretical costs of calcification (Anthony *et al.*, 2002; Allemand *et al.*, 2011). Other studies, however, use the enthalpy of combustion of protein to estimate the cost of synthesizing the protein organic matrix (Waldbusser *et al.*, 2013). This enthalpy value of 24.0 kJ (g protein)$^{-1}$ for the energy release from the catabolism of protein (Gnaiger, 1983) is an order-of-magnitude larger than the theoretical cost of PS [the minimum cost of PS is estimated to be between ~1 and ~5.0 J mg^{-1} (Buttery and Boorman, 1976; Webster, 1981; Pace and Manahan, 2007)]. Recent studies by Pan *et al.* (2015) of early developmental stages of sea urchins (larvae of *Strongylocentrotus purpuratus* undergoing calcification) have reported a cost of 2.4 ± 0.2 J (mg protein synthesized)$^{-1}$, that is independent of ocean acidification treatment. Larvae of *C. gigas* have a similar cost of PS that is close to theoretical minimum, at 2.1 ± 0.2 J (mg protein synthesized)$^{-1}$ (Lee *et al.*, 2016). Notably this metabolic cost of PS in larvae of *C. gigas* is fixed across genotype, phenotype, and environmental temperature, thereby simplifying bioenergetic calculations. In summary,

while 24 J of energy are made available through complete oxidative catabolism of a milligram of protein to carbon dioxide and ammonia, only ~2 J are required to synthesize the same mass of protein from pre-formed dietary amino acids (heterotrophic metabolism). Prior theoretical estimates of the energy required to form the proteinaceous matrix of shell that are based on enthalpic equivalents of biochemical combustion, or inflated values for the cost of PS, would substantially decrease.

Regarding the energy cost of calcification under adverse aragonite conditions, previous studies have suggested that under future scenarios of ocean acidification there will be an increased energy demand to meet the increased cost of calcification (Waldbusser *et al.*, 2013, 2016a,b). To construct accurate energy budgets, the rate of energy consumption (respiration) has to be known for a direct comparison to the rate of energy input from depletion of energy reserves (e.g. lipids). In our study, we present such an analysis and conclude that developing stages of *C. gigas* are not energy limited at aragonite undersaturation. We base this conclusion on the following analysis. First, there is no effect of aragonite saturation on the respiration rates of larvae (Figure 5a). Second, the rate of depletion of the major energy reserves of lipid and protein was not different between control and aragonite undersaturated-treated larvae (data in Results). Third, the amount of energy required to form the 56% shell not formed due to aragonite undersaturation could be fully supported by the available energy reserves in pre-feeding stages of larvae. This latter point is critical as it leads to the conclusion that shell formation in early stage larvae is not energy limited under aragonite undersaturation.

As above, the energy cost to calcify a unit mass of shell is estimated to be no more than 1.1 J (mg $CaCO_3$)$^{-1}$. What does change, however, is the amount of total energy required to accrete a given amount of shell when there is turnover (i.e. dissolution of shell); this additional cost can be calculated as follows. At a cost of 1.1 J (mg $CaCO_3$)$^{-1}$, the accretion of 74 ng of shell under control conditions (Figure 1b) requires 67% (80.4 μJ of 120 μJ) of total energy required during this period of development (Figures 5a and 7b). At aragonite undersaturation, during the same period of development studied, a larva only accreted 32 ng of shell (Figure 1b). The difference of 42 ng (74 – 32 ng) in decreased calcification would require an additional 46.2 μJ to grow the same shell mass as control larvae. Do early-stage larvae of *C. gigas* have sufficient energy reserves to meet this increased cost of shell accretion? If not, then energy limitation can reasonably be invoked as a causative factor in decreased shell formation at aragonite undersaturation. This extra "cost of living" (46.2 μJ) to maintain shell growth under adverse conditions of aragonite undersaturation is 166.2 μJ (120 + 46.2 μJ). As given in Figure 6, larvae have 204 μJ in protein, 126 μJ in TAGs, and 67 μJ in phospholipids for a total of 397 μJ in biochemical reserves—more than 2.4-times the energy required to sustain shell growth at aragonite undersaturation. Since larvae do not draw further upon these available energy reserves to meet the additional metabolic cost of maintaining shell formation under aragonite undersaturation (Figure 6), it appears that the observed 56% loss of shell mass is not energy related. Larval forms of marine invertebrates have considerable flexibility in how energy is allocated, as has been shown with up-regulation of mass-specific metabolic rate in response to environmental chemistry (Jaeckle and Manahan 1992; Leong and Manahan 1997; Pan *et al.*, 2015), such that if calcification at aragonite undersaturation necessitated increased ATP utilization, an increase in metabolic rate would have been apparent (and was not, Figure 5a). In addition, larvae of *C. gigas* have been shown to maintain their protein reserves in the absence of particulate food, while maintaining metabolic rates (Moran and Manahan, 2004). Presumably the ability of larvae to gain additional energy from the direct transport of dissolved organic material from seawater plays an important role in balancing energy budgets to support observed respiration rates. In summary, our analyses do not support a biochemical energy-reserve limitation component of the "kinetic-energetic hypothesis" (Waldbusser *et al.* 2013, 2015, 2016a,b). Our results do support, however, possible physical–chemical rate processes that impact kinetic constraints on calcification under ocean acidification, as demonstrated by decreased calcification rates at aragonite undersaturation (Figure 3b).

Physiological variation among larval families and adaptation to global ocean change

Adaptation to global change relies on selection of pre-existing, standing genetic variation within populations (Barrett and Schluter, 2008). Yet progress on the study of adaptation to global change in the ocean has been impeded by lack of marine model organisms with genetic and genomic resources (Applebaum *et al.*, 2014). Quantitative determination of genetic-based variation requires experimental studies, in which variance can be partitioned into environmental and genetic components (Lynch and Walsh, 1998). Although our experiments were not designed as a formal quantitative genetic study, we did analyse changes in calcification in different larval families produced by controlled crosses of adults from pedigreed families of the Pacific oyster, *C. gigas*. We found, most notably, a significant family-by-environmental interaction effect on shell length during first-shell formation at aragonite undersaturation (Table 2, Figure 1a and c). The impact of aragonite undersaturation among families ranged from no effect to more than a 20-μm decrease in shell length (0–28% change). These differences for the impact of aragonite undersaturation among larval families suggest the possibility that resilience to ocean acidification may differ among present-day genotypes. In the 2 × 2 male-by-female factorial cross of Trial-a (Table 1), the inbred 2 × 2 genotype (Family 1) showed the most resilience, while the 2 × 1 hybrid (Family 8) was one of the most sensitive families to aragonite undersaturation, more sensitive even than its 1 × 1 inbred parent (Family 6) and more so than the reciprocal hybrid 1 × 2 (Family 2). Significant differences among the paternal half-sibs in Trial-b (Families 3, 4, and 9) suggest additive genetic variance in resilience, but maternal effects or negative nuclear-cytoplasmic interaction (i.e. analysis of reciprocal hybrids) may also be part of standing genetic variation (Hedgecock and Davis, 2007). Further experiments involving pedigreed lines offer a quantitative genetic approach to study specific mechanisms that underlie shell growth phenotypic contrasts in response to ocean acidification (Figure 1c; Applebaum *et al.*, 2014).

In summary, we have developed a quantitative bioenergetic framework for evaluating possible trade-offs between the cost of calcification and other physiological processes that require energy during development (Figures 5 and 6). This framework is based on, first, defining the energy requirements for the major cellular-level ATP-consuming processes, and then placing these processes within the whole organism's energy budget (ATP metabolic "pie-chart"). The rapid developmental period of first-shell formation in larvae of *C. gigas* is a critical life-history stage, when six times

the organic mass (Figure 6a) is precipitated as inorganic shell (Figure 1b). Applying ATP equivalents to this stage of development has provided new insights into the bases of biological responses to the stress of aragonite undersaturation. We show that there was no increase in total energy expenditure at aragonite undersaturation, nor were larvae limited by their endogenous energy reserves of lipid and protein. Furthermore, energy allocation to PS was maintained, such that protein metabolic dynamics were not impacted. In other animals and life stages, the effects of experimental ocean acidification on cellular energy budgets may of course be different, but applying bioenergetics to the study of calcification in the context of development and growth will help to clarify the varied responses of calcifying marine biota to global ocean change.

Acknowledgements

We thank Charles Capron for technical assistance and to Xiaoshen Yin for assistance with genotyping. We thank Taylor Shellfish Farms (Shelton, Washington) for helping maintain the pedigreed lines used in this study. We thank also to the staff of the USC Wrigley Marine Science Center on Santa Catalina Island where culture-related experiments were completed.

Funding

This work was supported by a grant from the National Science Foundation (EF-1220587).

References

Allemand, D., Tambutté, É., Zoccola, D., and Tambutté, S. 2011. Coral calcification, cells to reefs. *In* Coral Reefs: An Ecosystem in Transition, pp. 119–150. Springer Netherlands, Dordrecht.

Andersson, A. J., and Gledhill, D. 2013. Ocean acidification and coral reefs: Effects on breakdown, dissolution, and net ecosystem calcification. Annual Review of Marine Science, 5: 321–348.

Anthony, K. R. N., Connolly, S. R., and Willis, B. L. 2002. Comparative analysis of energy allocation to tissue and skeletal growth in corals. Limnology and Oceanography, 47: 1417–1429.

Applebaum, S. L., Pan, T. C. F., Hedgecock, D., and Manahan, D. T. 2014. Separating the nature and nurture of the allocation of energy in response to global change. Integrative and Comparative Biology, 54: 284–295.

Bandstra, L., Hales, B., and Takahashi, T. 2006. High-frequency measurements of total CO_2: Method development and first oceanographic observations. Marine Chemistry, 100: 24–38.

Barrett, R.D.H., and Schluter, D. 2008. Adaptation from standing genetic variation. Trends in Ecology and Evolution, 23: 38–44.

Barton, A., Hales, B., Waldbusser, G. G., Langdon, C. J., and Feely, R. A. 2012. The Pacific oyster, *Crassostrea gigas*, shows negative correlation to naturally elevated carbon dioxide levels: implications for near-term ocean acidification effects. Limnology and Oceanography, 57: 698–710.

Barton, A., Waldbusser, G. G., Feely, R. A., et al. 2015. Impacts of coastal acidification on the Pacific Northwest shellfish industry and adaptation strategies implemented in response. Oceanography, 28: 146–159.

Belcher, A. M., Wu, X. H., Christensen, R. J., Hansma, P. K., Stucky, G. D., and Morse, D. E. 1996. Control of crystal phase switching and orientation by soluble mollusc-shell proteins. Nature, 381: 56–58.

Brunner, E. L., Prahl, F. G., Hales, B., and Waldbusser, G. G. 2016. A longitudinal study of Pacific oyster (*Crassostrea gigas*) larval development: isotope shifts during early shell formation reveal sublethal energetic stress. Marine Ecology Progress Series, 18: 109–123.

Buttery, P. J., and Boorman, K. N. 1976. The energetic efficiency of amino acid metabolism. *In* Protein Nutrition and Metabolism, pp. 197–206. Ed. by D. Cole, K. Boorman, P. Buttery, D. Lewis, R. Neale, and H. Swan. Butterworths, London.

Cornwall, C. E., and Hurd, C. L. 2016. Experimental design in ocean acidification research: problems and solutions. ICES Journal of Marine Science, 73: 572–581.

Curole, J. P., Meyer, E., Manahan, D. T., and Hedgecock, D. 2010. Unequal and genotype-dependent expression of mitochondrial genes in larvae of the Pacific oyster *Crassostrea gigas*. Biological Bulletin, 218: 122–131.

Cyronak, T., Schulz, K. G., and Jokiel, P. L. 2016a. Response to Waldbusser et al. (2016): "Calcium carbonate saturation state: on myths and this or that stories". ICES Journal of Marine Science, 73: 569–571.

Cyronak, T., Schulz, K. G., and Jokiel, P. L. 2016b. The Omega myth: what really drives lower calcification rates in an acidifying ocean. ICES Journal of Marine Science, 73: 558–562.

Davidson, E. H. 2010. The Regulatory Genome: Gene Regulatory Networks in Development and Evolution. Academic press, Burlington, San Diego, London.

Dickson, A. G., Sabine, C. L., and Christian, J. R. 2007. Guide to best practices for ocean CO_2 measurements. PICES Special Publication 3, Sydney, British Columbia, 191 pp.

Gallager, S. M., and Mann, R. 1986. Growth and survival of larvae of *Mercenaria mercenaria* (L.) and *Crassostrea virginica* (Gmelin) relative to broodstock conditioning and lipid content of eggs. Aquaculture, 56: 105–121.

Gaylord, B., Hill, T. M., Sanford, E., Lenz, E. A., Jacobs, L. A., Sato, K. N., Russell, A. D., and Hettinger, A. 2011. Functional impacts of ocean acidification in an ecologically critical foundation species. Journal of Experimental Biology, 214: 2586–2594.

Gnaiger, E. 1983. Calculation of energetic and biochemical equivalents of respiratory oxygen consumption. *In* Polarographic Oxygen Sesnors: Aquatic and Physiological Applications, pp. 337–345. Ed. by E. Gnaiger, and H. Forstner. Springer-Verlag, New York, NY.

Gobler, C. J., and Talmage, S. C. 2013. Short- and long-term consequences of larval stage exposure to constantly and ephemerally elevated carbon dioxide for marine bivalve populations. Biogeosciences, 10: 2241–2253.

Hales, B., Takahashi, T., and Bandstra, L. 2005. Atmospheric CO_2 uptake by a coastal upwelling system. Global Biogeochemical Cycles, 19: GB1009.

Hedgecock, D., and Davis, J. P. 2007. Heterosis for yield and crossbreeding of the Pacific oyster *Crassostrea gigas*. Aquaculture, 272: S17–S29.

Heinemann, A., Fietzke, J., Melzner, F., Böhm, F., Thomsen, J., Garbe-Schönberg, D., and Eisenhauer, A. 2012. Conditions of *Mytilus edulis* extracellular body fluids and shell composition in a pH-treatment experiment: acid-base status, trace elements and $\delta^{11}B$. Geochemistry, Geophysics, Geosystems, 13: Q01005.

His, E., and Maurer, D. 1988. Shell growth and gross biochemical composition of oyster larvae (*Crassostrea gigas*) in the field. Aquaculture 69: 185–194.

Hochachka, P. W., and Somero, G. N. 2002. Biochemical Adaptation: Mechanism and Process in Physiological Evolution. Oxford University Press, New York. 480 pp.

Hoegh-Guldberg, O., and Manahan, D. T. 1995. Coulometric measurement of oxygen consumption during development of marine invertebrate embryos and larvae. Journal of Experimental Biology, 198: 19–30.

Hohagen, J., and Jackson, D. J. 2013. An ancient process in a modern mollusc: Early development of the shell in *Lymnaea stagnalis*. BMC Developmental Biology, 13: 1–13.

Hurlbert, S. H. 1984. Pseudoreplication and the design of ecological field experiments. Ecological Monographs, 54: 187–211.

Jaeckle, W. B., and Manahan, D. T. 1989. Growth and energy imbalance during the development of a lecithotrophic molluscan larva *Haliotis rufescens*. Biological Bulletin, 177: 237–346.

Jaeckle, W. B., and Manahan, D. T. 1992. Experimental manipulations of the organic chemistry of seawater: implications for studies of energy budgets in marine invertebrate larvae. Journal of Experimental Marine Biology and Ecology, 156: 273–284.

Johnstone, M. B., Gohad, N. V., Falwell, E. P., Hansen, D. C., Hansen, K. M., and Mount, A. S. 2015. Cellular orchestrated biomineralization of crystalline composites on implant surfaces by the eastern oyster, *Crassostrea virginica* (Gmelin, 1791). Journal of Experimental Marine Biology and Ecology, 463: 8–16.

Kniprath, E. 1981. Ontogeny of the molluscan shell field: A review. Zoologica Scripta, 10: 61–79.

Kurihara, H., Kato, S., and Ishimatsu, A. 2007. Effects of increased seawater pCO_2 on early development of the oyster *Crassostrea gigas*. Aquatic Biology, 1: 91–98.

Lee, J. W., Applebaum, S. L., and Manahan, D. T. 2016. Metabolic cost of protein synthesis in larvae of the Pacific oyster (*Crassostrea gigas*) is fixed across genotype, phenotype, and environmental temperature. Biological Bulletin, 230: 175–187.

Leong, P. K. K., and Manahan, D. T. 1997. Metabolic importance of Na^+/K^+-ATPase activity during sea urchin development. Journal of Experimental Biology, 200: 2881–2892.

Lowenstam, H. A., and Margulis, L. 1980. Calcium regulation and the appearance of calcareous skeletons in the fossil record. *In* The Mechanisms of Biominerlaization in Animals and Plants, pp. 289–300. Ed. by M. Omori, and N. Watabe. Tokai University Press, Tokyo.

Lowenstam, H. A., and Weiner, S. 1989. On Biomineralization. Oxford University Press, New York. 324 pp.

Lynch, M., and Walsh, B. 1998. Genetics and Analysis of Quantitative Traits. Sinauer Associates, Inc., Sunderalnd. 980 pp.

Mann, S. 2001. Biomineralization: Principles and Concepts in Bioinorganic Materials Chemistry. Oxford University Press, New York. 198 pp.

Mao, L.-B., Gao, H.-L., Yao, H.-B., et al. 2016. Synthetic nacre by predesigned matrix-directed mineralization. Science, 354: 107–110.

Marsh, A. G., and Manahan, D. T. 1999. A method for accurate measurements of the respiration rates of marine invertebrate embryos and larvae. Marine Ecology Progress Series, 184: 1–10.

McGilvery, R. 1979. Biochemistry: A Functional Approach. WB Saunders, Philadelphia. 769 pp.

Manahan, D. T. 1983a. The uptake of dissolved glycine following fertilization of oyster eggs (*Crassostrea gigas* Thunberg). Journal of Experimental Marine Biology and Ecology, 68: 53–58.

Manahan, D. T. 1983b. The uptake and metabolism of dissolved amino acids by bivalve larvae. Biological Bulletin, 164: 236–250.

Manahan, D. T., and Crisp, D. J. 1983. Autoradiographic studies on the uptake of dissolved amino acids by bivalve larvae. Journal of the Marine Biological Association of the United Kingdom, 63: 673–682.

Manahan, D. T., Wright, S. H., Stephens, G. C., and Rice, M. A. 1982. Transport of dissolved amino acids by the mussel *Mytilus edulis*: demonstration of net uptake from natural seawater. Science, 215: 1253–1255.

Melzner, F., Stange, P., Trübenbach, K., et al. 2011. Food supply and seawater pCO_2 impact calcification and internal shell dissolution in the blue mussel *Mytilus edulis*. PLoS One, 6: e24223.

Meyer, E., and Manahan, D. T. 2010. Gene expression profiling of genetically-determined growth variation in bivalve larvae (*Crassostrea gigas*). Journal of Experimental Biology, 213: 749–758.

Moran, A. L., and Manahan, D. T. 2004. Physiological recovery from prolonged "starvation" in larvae of the Pacific oyster *Crassostrea gigas*. Journal of Experimental Marine Biology and Ecology, 306: 17–36.

Mount, A. S., Wheeler, A. P., Paradkar, R. P., and Snider, D. 2004. Hemocyte-mediated shell mineralization in the eastern oyster. Science, 304: 297–300.

Pace, D. A., and Manahan, D. T. 2006. Fixed metabolic costs for highly variable rates of protein synthesis in sea urchin embryos and larvae. Journal of Experimental Biology, 209: 158–170.

Pace, D. A., Marsh, A. G., Leong, P. K. K., Green, A. J., Hedgecock, D., and Manahan, D. T. 2006. Physiological bases of genetically determined variation in growth of marine invertebrate larvae: A study of growth heterosis in the bivalve *Crassostrea gigas*. Journal of Experimental Marine Biology and Ecology, 335: 188–209.

Pace, D. A., and Manahan, D. T. 2007. Cost of protein synthesis and energy allocation during development of Antarctic sea urchin embryos and larvae. Biological Bulletin, 212: 115–129.

Palmer, A. R. 1992. Calcification in marine molluscs: How costly is it?. Proceedings of the National Academy of Sciences of the United States of America, 89: 1379–1382.

Pan, T. C. F., Applebaum, S. L., Lentz, B. A., and Manahan, D. T. 2016. Predicting phenotypic variation in growth and metabolism of marine invertebrate larvae. Journal of Experimental Marine Biology and Ecology, 483: 64–73.

Pan, T. C. F., Applebaum, S. L., and Manahan, D. T. 2015. Experimental ocean acidification alters the allocation of metabolic energy. Proceedings of the National Academy of Sciences of the United States of America, 112: 4696–4701.

Pequignat, E. 1973. A kinetic and autoradiographic study of the direct assimilation of amino acids and glucose by organs of the mussel *Mytilus edulis*. Marine Biology, 19: 227–244.

Piez, K. A. 1961. Amino acid composition of some calcified proteins. Science 134: 841–842.

Ponder, W. F., and Lindberg, D. R. 2008. Phylogeny and Evolution of the Mollusca. University of California Press, Berkeley and Los Angeles. 469 p.

Quinn, G. P., and Keough, M. J. 2002. Experimental Design and Data Analysis for Biologists. Cambridge University Press, Cambridge. 553 pp.

Raff, R. A., and Kaufman, T. C. 1991. Embryos, Genes, and Evolution: Developmental-Genetic Basis of Evolutionary Change. Indiana University Press, Bloomington. 424 pp.

Simkiss, K., and Wilbur, K. 1989. Biomineralization: Cell Biology and Mineral Deposition. Academic Press, San Diego. 337 pp.

Sokolova, I. M., Frederich, M., Bagwe, R., Lannig, G., and Sukhotin, A. A. 2012. Energy homeostasis as an integrative tool for assessing limits of environmental stress tolerance in aquatic invertebrates. Marine Environmental Research, 79: 1–15.

Stenzel, H. 1963. Aragonite and calcite as constituents of adult oyster shells. Science, 142: 232–233.

Stenzel, H. B. 1964. Oysters: composition of the larval shell. Science, 145: 155–156.

Sun, X., Shin, G., and Hedgecock, D. 2015. Inheritance of high-resolution melting profiles in assays targeting single nucleotide polymorphisms in protein-coding sequences of the Pacific oyster *Crassostrea gigas*: Implications for parentage assignment of experimental and commercial broodstocks. Aquaculture 437: 127–139.

Thompson, D. W. 1942. On Growth and Form. Dover Publications. 1116 pp.

Thomsen, J., Casties, I., Pansch, C., Körtzinger, A., and Melzner, F. 2013. Food availability outweighs ocean acidification effects in juvenile *Mytilus edulis*: Laboratory and field experiments. Global Change Biology, 19: 1017–1027.

Thomsen, J., Haynert, K., Wegner, K. M., and Melzner, F. 2015. Impact of seawater carbonate chemistry on the calcification of marine bivalves. Biogeosciences, 12: 4209–4220.

Waldbusser, G. G., Bergschneider, H., and Green, M. A. 2010. Size-dependent pH effect on calcification in post-larval hard clam *Mercenaria* spp. Marine Ecology Progress Series, 417: 171–182.

Waldbusser, G. G., Brunner, E. L., Haley, B. A., Hales, B., Langdon, C. J., and Prahl, F. G. 2013. A developmental and energetic basis linking larval oyster shell formation to acidification sensitivity. Geophysical Research Letters, 40: 2171–2176.

Waldbusser, G. G., Hales, B., Langdon, C. J., et al. 2014. Saturation-state sensitivity of marine bivalve larvae to ocean acidification. Nature Climate Change, 5: 273–280.

Waldbusser, G. G., Hales, B., Langdon, C. J., et al. 2015. Ocean acidification has multiple modes of action on bivalve larvae. PLoS One, 10: e0128376.

Waldbusser, G. G., Gray, M. W., Hales, B., et al. 2016a. Slow shell building, a possible trait for resistance to the effects of acute ocean acidification. Limnology and Oceanography, 61: 1969–1983.

Waldbusser, G. G., Hales, B., and Haley, B. A. 2016b. Calcium carbonate saturation state: on myths and this or that stories. ICES Journal of Marine Science, 73: 563–568.

Webster, A. 1981. The energetic efficiency of metabolism. Proceedings of the Nutrition Society, 40: 121–128.

Wright, S. H., and Secomb, T. W. 1986. Epithelial amino acid transport in marine mussels: role in net exchange of taurine between gills and sea water. Journal of Experimental Biology, 121: 251–270.

Handling editor: Howard Browman